Single-cell landscape of innate and acquired drug resistance in acute myeloid leukemia

Rebekka Wegmann[*,1], Ximena Bonilla[*,2], Ruben Casanova[*,3], Stéphane Chevrier[*,3], Ricardo Coelho[*,4], Cinzia Esposito[*,5], Joanna Ficek-Pascual[*,2], Sandra Goetze[*,6,7,8], Gabriele Gut[*,5], Francis Jacob[*,4], Andrea Jacobs[*,3], Jack Kuipers[*,9], Ulrike Lischetti[*,4], Julien Mena[*,1], Emanuela S. Milani[*,6], Michael Prummer[*,8,10], Jacobo Sarabia Del Castillo[*,5], Franziska Singer[*,8,10], Sujana Sivapatham[*,3], Nora C. Toussaint[*,8,10,11], Oliver Vilinovszki[*,12], Mattheus H. E. Wildschut[*,1,6,12], Tharshika Thavayogarajah[12], Disha Malani[13], The TumorProfiler Consortium, Rudolf Aebersold[#,1], Marina Bacac[#,14], Niko Beerenwinkel[#,8,9], Christian Beisel[#,9], Bernd Bodenmiller[#,3,6], Viola Heinzelmann-Schwarz[#,4], Viktor H. Koelzer[#,15,16], Mitchell P. Levesque[#,17], Holger Moch[#,15,16], Lucas Pelkmans[#,5], Gunnar Rätsch[#,2,8,18], Markus Tolnay[#,19], Andreas Wicki[#,12,16], Bernd Wollscheid[#,6], Markus G. Manz[#,✉,12], Berend Snijder[#,✉,1,8], Alexandre P. A. Theocharides[#,✉,12]

* These authors contributed equally
\# These authors jointly supervised this work
✉ Correspondence to:
markus.manz@usz.ch, snijder@imsb.biol.ethz.ch, or alexandre.theocharides@usz.ch

1 Institute of Molecular Systems Biology, Department of Biology, ETH Zurich, Switzerland
2 Department of Computer Science, ETH Zurich, Switzerland
3 Department of Quantitative Biomedicine, University of Zurich, Switzerland
4 Department of Biomedicine, University Hospital Basel and University of Basel, Switzerland
5 Institute of Molecular Life Sciences, University of Zurich, Switzerland
6 Department of Health Sciences and Technology, ETH Zurich, Switzerland
7 ETH PHRT Swiss Multi-Omics Center (SMOC), Switzerland
8 SIB Swiss Institute of Bioinformatics
9 Department of Biosystems Science and Engineering, ETH Zurich, Switzerland
10 NEXUS Personalized Health Technologies, ETH Zurich, Switzerland
11 Current address: Swiss Data Science Center, ETH Zürich, Zurich, Switzerland
12 Department of Medical Oncology and Hematology, University Hospital Zurich, Switzerland
13 Harvard Medical School and Dana-Farber Cancer Institute, Boston, USA
14 Roche Pharmaceutical Research and Early Development, Roche Innovation Center Zurich, Switzerland
15 Department of Pathology and Molecular Pathology, University Hospital Zurich, Switzerland
16 University of Zurich, Faculty of Medicine, Switzerland
17 University Hospital Zurich, Department of Dermatology, Switzerland
18 AI Center at ETH Zurich, Switzerland
19 Institute of Medical Genetics and Pathology, University Hospital Basel, Switzerland

Supplementary material

Contents

Supplementary Case Studies

TP008

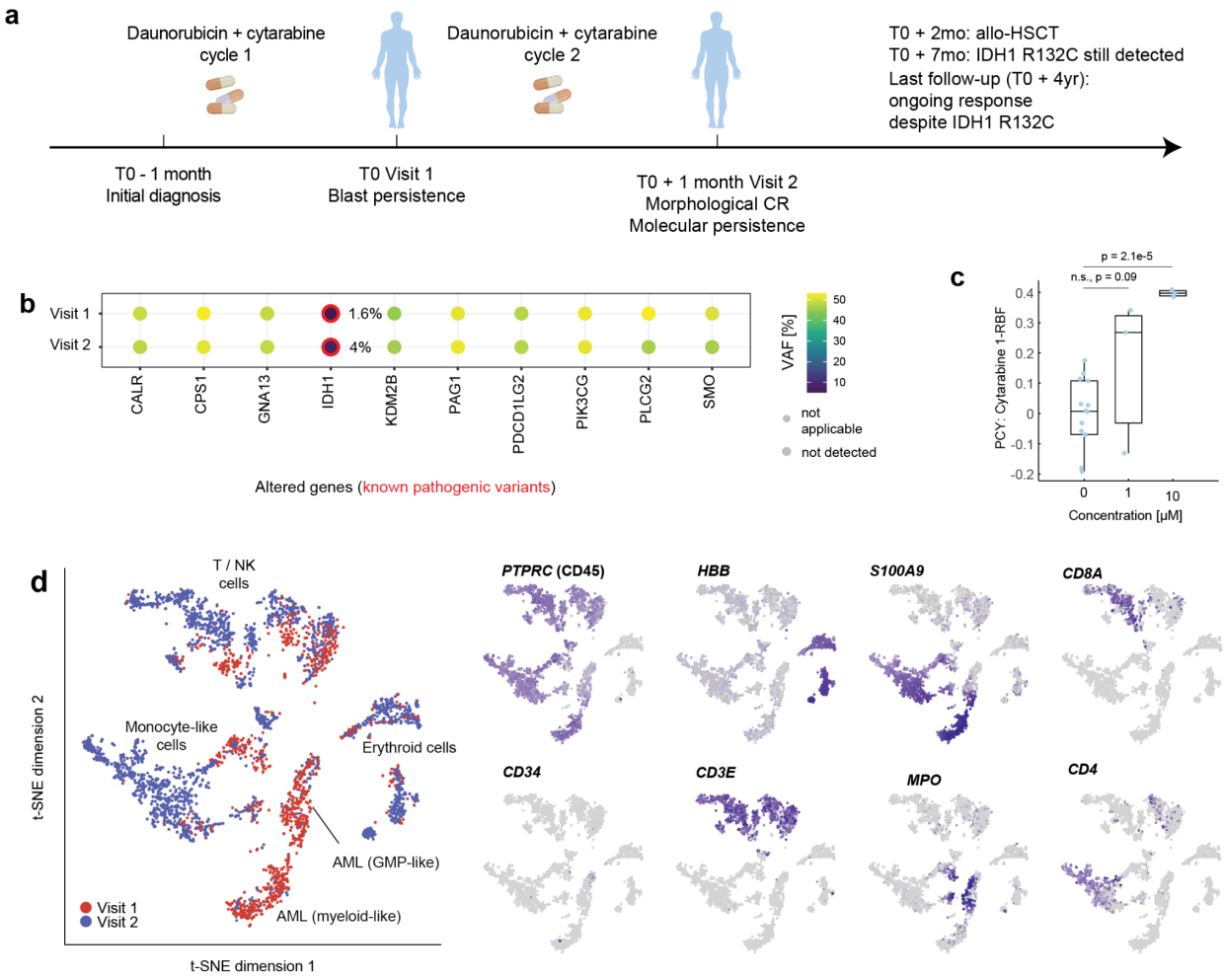

Supplementary Figure 1. a: Schematic of the clinical course of patient TP008. **b**: Variant allele frequencies from FoundationOne Heme for genomic alterations detected in at least one patient sample. **c**: Pharmacoscopy (PCY) *ex vivo* response (1-relative blast fraction, RBF) for different concentrations of cytarabine. Dots correspond to individual replicate wells (n = 3 per drug concentration, n = 16 for DMSO control). *P* values from Tukey's HSD test. Box plots indicate the median (horizontal line) and 25% and 75% ranges (box) and whiskers indicate the 1.5x interquartile range above or below the box. **d**: t-SNE calculated on the batch-corrected expression values of all cells measured by scRNA-seq (visit 1: 960 cells, visit 2: 2343 cells). Regions in the t-SNE are annotated with the most abundant cell type, small plots on the side show cell type specific marker gene expression (darker color = higher expression).

Patient TP008 was diagnosed with AML, NOS one month prior to the first study visit. A pathogenic *IDH1* R132C mutation was detected at this point with a variant allele frequency of around 20%. The patient then received one cycle of induction chemotherapy with daunorubicin + cytarabine, which led to a reduction in AML blasts, but complete response was not achieved. At this time point, the first TuPro sample was taken and analyzed **(Supplementary Figure 1a**). FoundationOne Heme confirmed the persistence of the *IDH1* R132C mutation in the bone marrow (**Supplementary Figure 1b**). PCY analysis highlighted strong on-target effects for cytarabine (**Supplementary Figure 1c**). scRNAseq identified 40% of AML blasts in the bone marrow sample at the first visit, mostly subclassified as GMP- and myeloid-like AML with very low expression of *CD34* (**Supplementary Figure 1d**). In addition, more mature myeloid cells and a considerable fraction (25%) of T-cells were also present. After the first chemotherapy cycle, the patient received a second cycle of induction chemotherapy and a complete remission was achieved. However, the *IDH1* R132C mutation persisted and the variant allele frequency even increased compared to the first visit (**Supplementary Figure 1b**). Consistent with the morphological complete remission, scRNA-seq identified almost complete absence (<5%) of AML blasts in the second sample, which was mostly composed of T/NK cells (40%), monocyte-like cells (40%) and erythroid cells (16%). The patient received an allo-HSCT after the second chemotherapy cycle, Interestingly, *IDH1* R132C persisted at low frequencies after allo-HSCT, a finding previously reported in the literature [1]. The patient remained in complete remission afterwards.

TP019

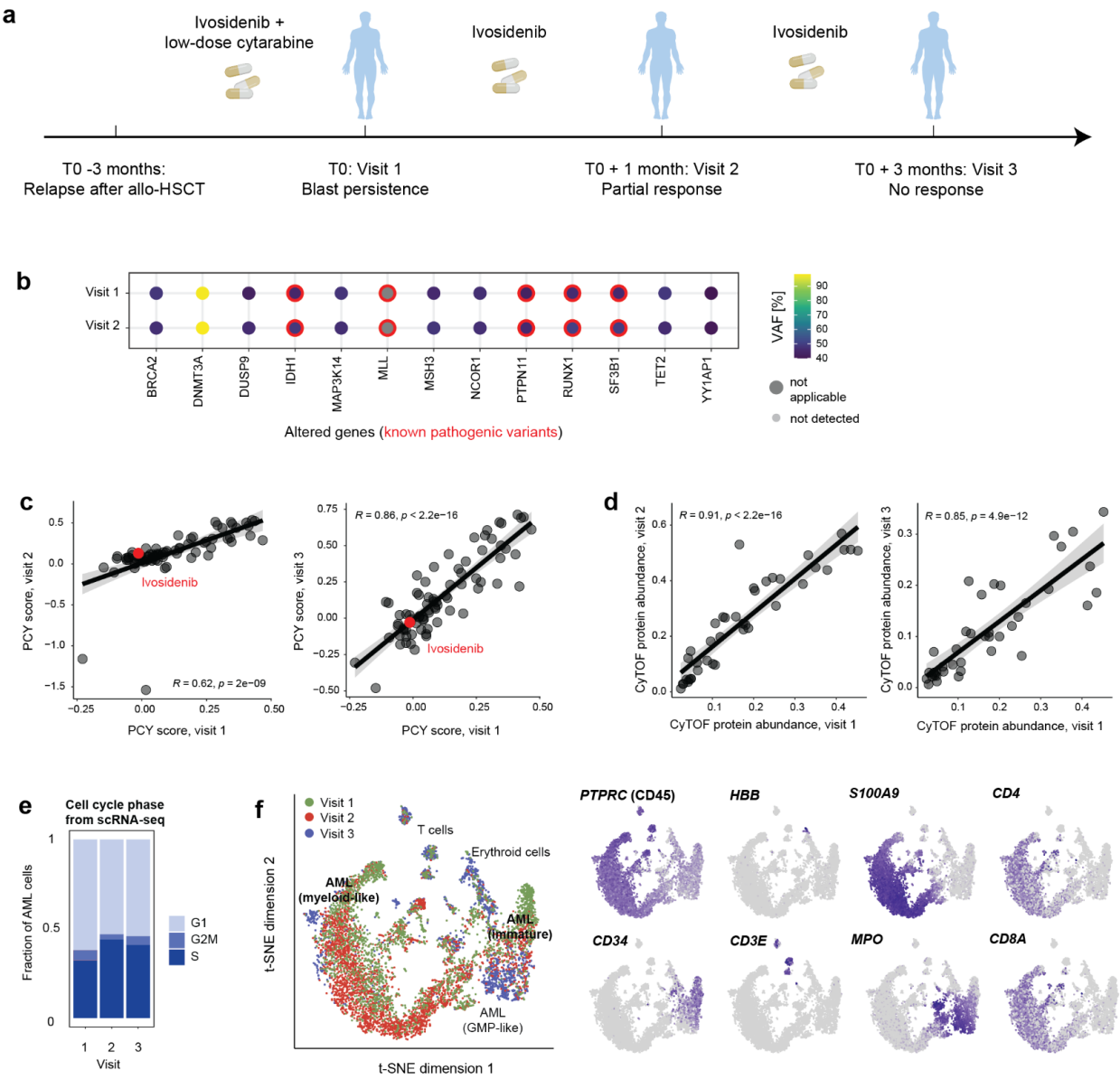

Supplementary Figure 2. a: Schematic of the clinical course of patient TP019. **b**: Variant allele frequencies from FoundationOne Heme for genomic alterations detected in at least one patient sample. **c**: Correlation of PCY scores between visit 1 and visits 2 and 3, respectively. The red dot highlights ivosidenib, which consistently shows no effect (PCY-score = 0) ex vivo. **d:** Correlation of CyTOF marker profiles (aggregated protein abundance across all AML cells) between visit 1 and visits 2 and 3, respectively. Lines and shaded areas in (c) and (d) correspond to a linear regression fit with 95% confidence bands, *P* values (two-sided t-test) and Pearson's *R* are indicated. **e:** Fraction of AML cells predicted to be in cell cycle phases G1, G2/M or S based on scRNA-seq. **f**: t-SNE calculated on the batch-corrected expression values of all cells measured by scRNA-seq (visit 1: 2380 cells, visit 2: 3614 cells, visit 3: 1781 cells). Regions in the t-SNE are annotated with the most abundant cell type, small plots on the side show cell type specific marker gene expression (darker color = higher expression).

Patient TP019 was initially diagnosed with myelodysplastic syndrome (MDS) with excess blasts (MDS-EB2). The patient relapsed after allo-HSCT 14 months after initial diagnosis, and presented with AML at relapse. The relapse was initially treated with decitabine + venetoclax. The therapy was then switched to ivosidenib and low-dose cytarabine due to intolerance to decitabine + venetoclax. A first TuPro sample was collected three months after relapse, and two follow-up biopsies were analyzed one and three months later, respectively (**Supplementary Figure 2a**). Throughout this time, the patient was treated with ivosidenib. Variant allele frequencies of pathogenic mutations (*IDH1* R132C, *TET2* D1075fs*7, *KMT2A (MLL)* partial tandem duplication (exons 2-10), *PTPN11* G503A, *RUNX1* R166*, and *SF3B1* H662D) remained constant during the first two visits, no FoundationOne was done at the third visit (**Supplementary Figure 2b**). PCY scores were highly correlated between visits (**Supplementary Figure 2c**), indicating no change in the drug sensitivity of the blast cells. Ivosidenib showed no effect *ex vivo* (PCY score around 0). This was consistent with the CyTOF analysis reporting highly similar protein expression across time points (**Supplementary Figure 2d**). scRNA-seq also showed no change in blast cell cycle state (**Supplementary Figure 2e**), and identified mostly AML blasts with high proportion of myeloid-like AML cells across visits (**Supplementary Figure 2f**).

TP024

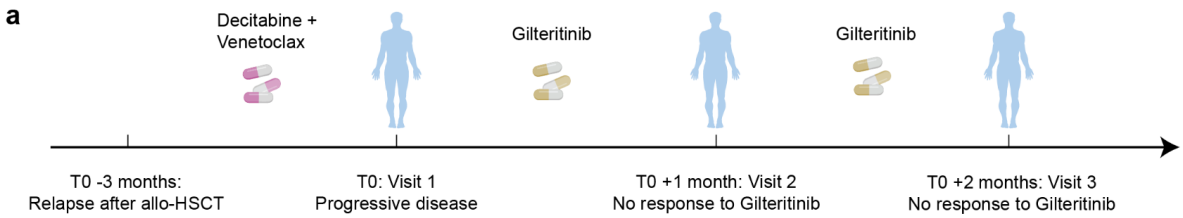
a
Decitabine +
Venetoclax
Gilteritinib
Gilteritinib
T0 -3 months:
Relapse after allo-HSCT
T0: Visit 1
Progressive disease
T0 +1 month: Visit 2
No response to Gilteritinib
T0 +2 months: Visit 3
No response to Gilteritinib

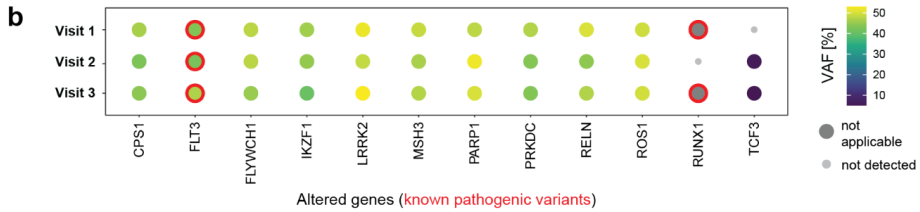
b
Visit 1
Visit 2
Visit 3
CPS1
FLT3
FLYWCH1
IKZF1
LRRK2
MSH3
PARP1
PRKDC
RELN
ROS1
RUNX1
TCF3
Altered genes (known pathogenic variants)
VAF [%]
50
40
30
20
10
not applicable
not detected

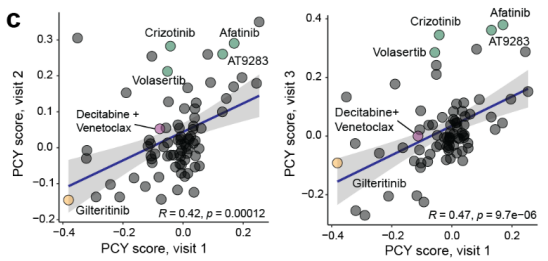
c
PCY score, visit 2
PCY score, visit 1
Crizotinib
Afatinib
AT9283
Volasertib
Decitabine +
Venetoclax
Gilteritinib
R = 0.42, p = 0.00012
PCY score, visit 3
PCY score, visit 1
R = 0.47, p = 9.7e−06

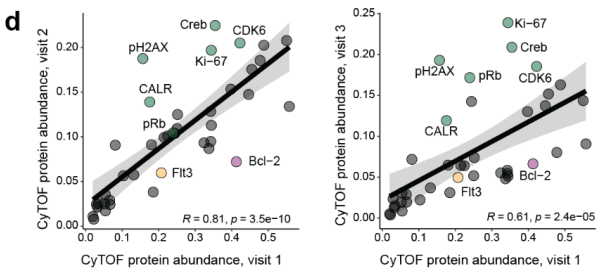
d
CyTOF protein abundance, visit 2
CyTOF protein abundance, visit 1
Creb
CDK6
pH2AX
Ki−67
CALR
pRb
Bcl−2
Flt3
R = 0.81, p = 3.5e−10
CyTOF protein abundance, visit 3
CyTOF protein abundance, visit 1
R = 0.61, p = 2.4e−05

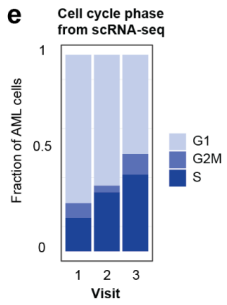
e
Cell cycle phase
from scRNA-seq
Fraction of AML cells
G1
G2M
S
Visit

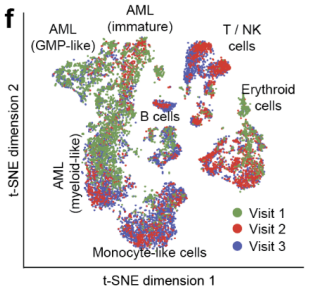
f
AML
(GMP-like)
AML
(immature)
T / NK
cells
Erythroid
cells
B cells
AML
(myeloid-like)
Monocyte-like cells
Visit 1
Visit 2
Visit 3
t-SNE dimension 2
t-SNE dimension 1

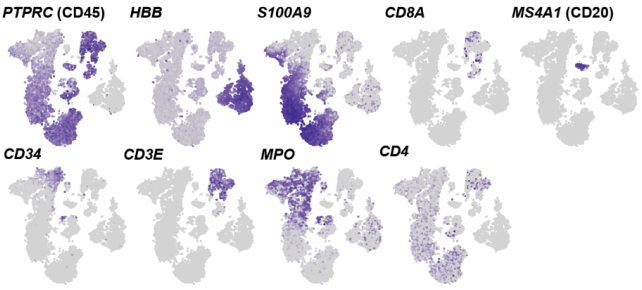
PTPRC (CD45)
HBB
S100A9
CD8A
MS4A1 (CD20)
CD34
CD3E
MPO
CD4

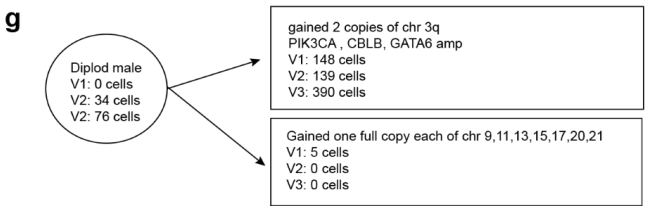
g
Diplod male
V1: 0 cells
V2: 34 cells
V2: 76 cells
gained 2 copies of chr 3q
PIK3CA , CBLB, GATA6 amp
V1: 148 cells
V2: 139 cells
V3: 390 cells
Gained one full copy each of chr 9,11,13,15,17,20,21
V1: 5 cells
V2: 0 cells
V3: 0 cells

Supplementary Figure 3. a: Schematic of the clinical course of patient TP024. **b**: Variant allele frequencies from FoundationOne Heme for genomic alterations detected in at least one patient sample. A *FLT3*-ITD (K602_W603insPWSK) mutation was detected at all visits. **c**: Correlation of PCY scores between visit 1 and visits 2 and 3, respectively. The colored dots highlight the previous treatment (decitabine + venetoclax) the treatment following the first visit (gilteritinib), as well as treatments that show increased sensitivity in visits 2 and 3 compared to visit 1 (green dots). **d**: Correlation of CyTOF marker profiles (aggregated protein abundance across all AML cells) between visit 1 and visits 2 and 3, respectively. Colored dots highlight the targets of previous (Bcl-2) and current (Flt-3) therapies. Dots highlighted in green correspond to proteins whose abundance increased in visits 2 and 3 relative to visit 1. Lines and shaded areas in (c) and (d) correspond to a linear regression fit with 95% confidence bands. *P* values (two-sided t-test) and Pearson's *R* are indicated. **e:** Fraction of AML cells predicted to be in cell cycle phases G1, G2/M or S based on scRNA-seq. **f**: t-SNE calculated on the batch-corrected expression values of all cells measured by scRNA-seq (visit 1: 3130 cells, visit 2: 3119 cells, visit 3: 6019 cells). Regions in the t-SNE are annotated with the most abundant cell type, small plots on the side show cell type specific marker gene expression (darker color = higher expression). **g**: Inferred cellular hierarchy based on copy number variations identified by scDNA-seq.

Patient TP024 was diagnosed with therapy-related MDS-EB2, which then rapidly progressed to AML. After an initial response to decitabine, the patient was treated by allo-HSCT and remained in remission for 7 months. He relapsed 3 months before the first study visit and treatment with decitabine + venetoclax was initiated, but AML progressed under this therapy (**Supplementary Figure 3a**). FoundationOne Heme identified a *FLT3*-ITD mutation, as well as a loss of exons 3-7 in *RUNX1*. The patient was then switched to gilteritinib after the first TuPro visit and treated throughout the study, however, the *FLT3* mutation persisted over time (**Supplementary Figure 3b**). Consistent with this lack of clinical sensitivity, PCY analysis revealed low *ex vivo* sensitivity to decitabine + venetoclax as well as gilteritinib in all samples. However, PCY highlighted an increase in *ex vivo* sensitivity to afatinib, crizotinib, volasertib and the combined aurora kinase / JAK inhibitor AT9283 over the course of the three time points (**Supplementary Figure 3c**). Potentially explaining the altered *ex vivo* drug sensitivity pattern, CyTOF reported elevated levels of proteins related to cell proliferation (pRb, Ki67, CDK6), DNA damage (pH2AX) and JAK/STAT signaling (CALR) (**Supplementary Figure 3d**). This increase in proliferation was confirmed by scRNA-seq analysis of predicted cell cycle phases in AML blasts, which went from 25% of cells in S or G2M phase in the first sample to almost 50% in the sample collected at visit 3 (**Supplementary Figure 3e**). scRNA-seq identified a majority of blasts among all cells in all visits, spanning the full spectrum from HSC-like to myeloid-like AML cells, with myeloid-like being the most abundant subtype. Interestingly, HSC-like cells were more abundant in visit 1, while samples from visits 2 and 3 contained higher fraction of myeloid-like AMl cells, monocyte-like and erythroid cells as well as other nonmalignant cells such as T cells and B cells that were almost entirely absent at visit 1 (**Supplementary Figure 3f**). scDNA-seq analysis identified one major clone, characterized by a gain of two copies of chromosome 3q, resulting in an amplification of CBLB, GATA2 and PIK3CA. Consistent with the increased fraction of nonmalignant cells identified by scRNA-seq, scDNA-seq detected no diploid cells at visit 1, but at visits 2 and 3, there were around 20% of cells present without any CNVs (**Supplementary Figure 3g**).

TP025

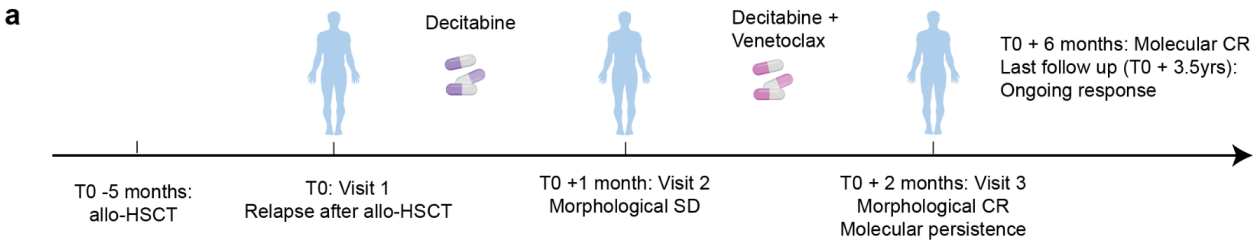
a
Decitabine
Decitabine +
Venetoclax
T0 + 6 months: Molecular CR
Last follow up (T0 + 3.5yrs):
Ongoing response
T0 -5 months:
allo-HSCT
T0: Visit 1
Relapse after allo-HSCT
T0 +1 month: Visit 2
Morphological SD
T0 + 2 months: Visit 3
Morphological CR
Molecular persistence

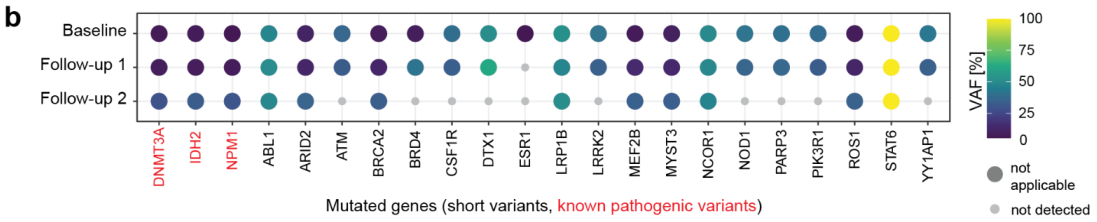
b
Baseline
Follow-up 1
Follow-up 2
DNMT3A
IDH2
NPM1
ABL1
ARID2
ATM
BRCA2
BRD4
CSF1R
DTX1
ESR1
LRP1B
LRRK2
MEF2B
MYST3
NCOR1
NOD1
PARP3
PIK3R1
ROS1
STAT6
YY1AP1
Mutated genes (short variants, known pathogenic variants)
VAF [%]
100
75
50
25
0
not applicable
not detected

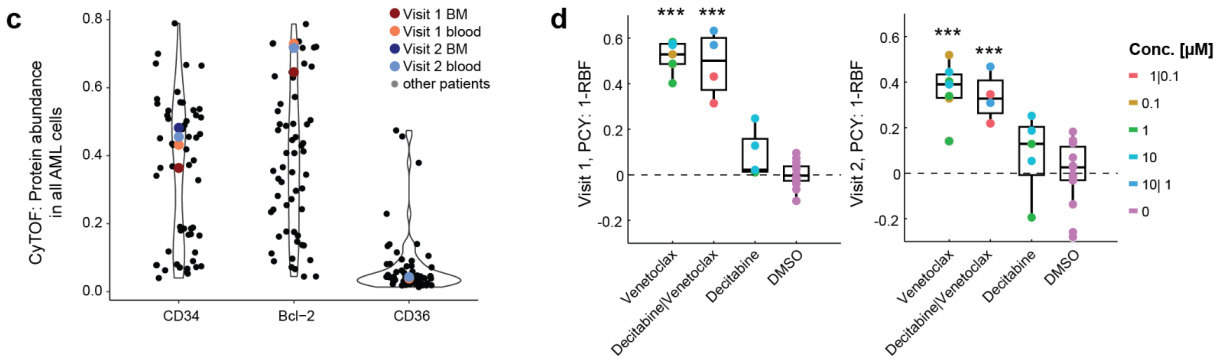
c
CyTOF: Protein abundance in all AML cells
Visit 1 BM
Visit 1 blood
Visit 2 BM
Visit 2 blood
other patients
CD34
Bcl−2
CD36
d
Visit 1, PCY: 1-RBF
Visit 2, PCY: 1-RBF
***
Venetoclax
Decitabine|Venetoclax
Decitabine
DMSO
Conc. [µM]
1|0.1
0.1
1
10
10| 1
0

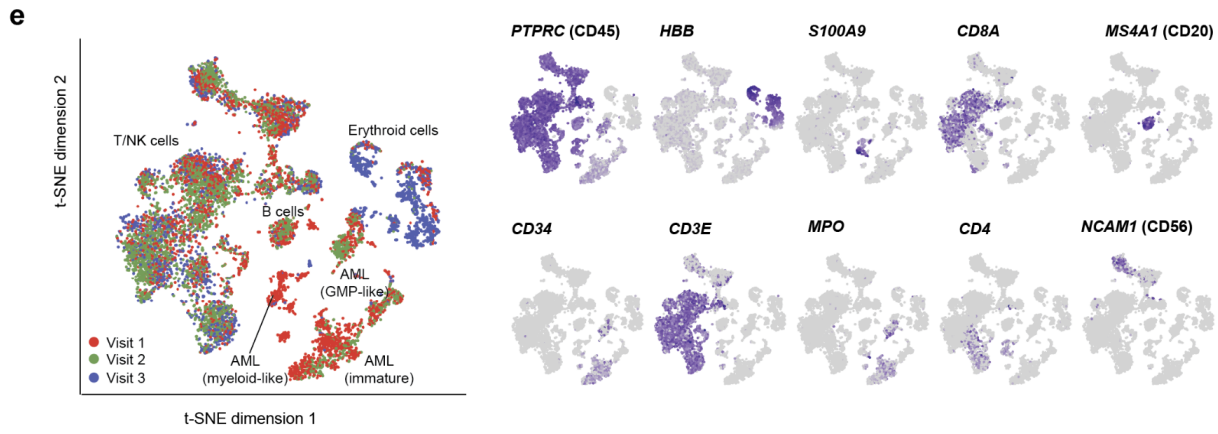
e
t-SNE dimension 2
t-SNE dimension 1
T/NK cells
Erythroid cells
B cells
AML
(GMP-like)
AML
(myeloid-like)
AML
(immature)
Visit 1
Visit 2
Visit 3
PTPRC (CD45)
HBB
S100A9
CD8A
MS4A1 (CD20)
CD34
CD3E
MPO
CD4
NCAM1 (CD56)

Supplementary Figure 4. a: Schematic of the clinical course of patient TP025. **b**: Variant allele frequencies from FoundationOne Heme for genomic alterations detected in at least one patient sample. **c**: Expression of CD34, Bcl-2 and CD36 by CyTOf. Black dots correspond to all samples in the cohort, colored dots mark samples from patient TP025. **d**: PCY responses (1-RBF) for decitabine, venetoclax, and decitabine + venetoclax at visits 1 & 2. *** P < 0.001, right-tailed Student's t-test comparing drug treated wells (all concentrations) to DMSO controls. Dots correspond to replicate wells (n = 4 or 5 per drug, n = 15 for DMSO ocntrol), box-plots as in Supplementary Figure 1c. **e:** t-SNE calculated on the batch-corrected expression values of all cells measured by scRNA-seq (visit 1: 3830 cells, visit 2: 3635 cells, visit 3: 2379 cells). Regions in the t-SNE are annotated with the most abundant cell type, small plots on the side show cell type specific marker gene expression (darker color = higher expression).

Patient TP025 was initially diagnosed with *NPM1* mutated AML. He initially responded to induction chemotherapy and received an allo–HSCT, but relapsed after 5 months, at which point the first TuPro sample was obtained. After the first visit, the patient started treatment with decitabine, resulting in no response at visit 2, after which venetoclax was added to the therapy and led to a complete remission (**Supplementary Figure 4a**). FoundationOne confirmed the presence of an *NPM1* W288fs*12 mutation, and also detected mutations in *DNMT3A* and *IDH2*. These mutations were detected at all time points, even after complete morphological remission. However, they were absent in a later follow-up sample that was not part of the study, suggesting that they likely originated from remaining dying blast cells or potentially from differentiated myeloid cells that originated from the mutated progenitors (**Supplementary Figure 4b**). Consistent with the clinical course of the patient, CyTOF analysis indicated high expression of CD34 and Bcl-2 in the AML blasts (**Supplementary Figure 4c**), and PCY showed on-target responses of the patient's AML cells to venetoclax and the combination of decitabine + venetoclax *ex vivo* (**Supplementary Figure 4d**). scRNA-seq analysis identified the presence of immature CD34 positive AML blasts at visits 1 and 2, which were all cleared at visit 3. Interestingly, erythroid cells were mainly detected in the sample at visit 3, potentially indicating the restoration of a healthy bone marrow environment (**Supplementary Figure 4e**).

TP030

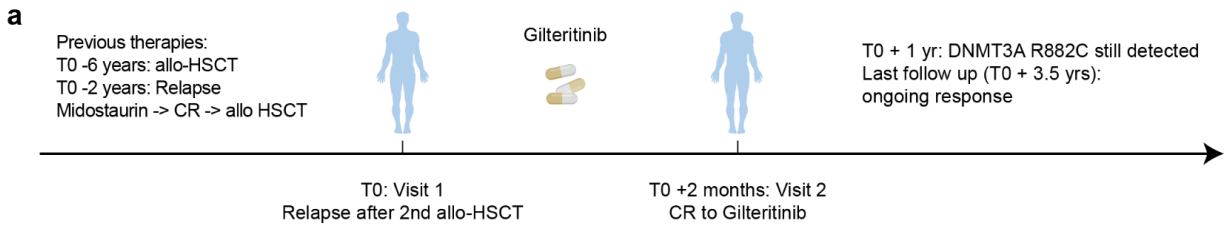
a
Previous therapies:
T0 -6 years: allo-HSCT
T0 -2 years: Relapse
Midostaurin -> CR -> allo HSCT
Gilteritinib
T0 + 1 yr: DNMT3A R882C still detected
Last follow up (T0 + 3.5 yrs):
ongoing response
T0: Visit 1
Relapse after 2nd allo-HSCT
T0 +2 months: Visit 2
CR to Gilteritinib

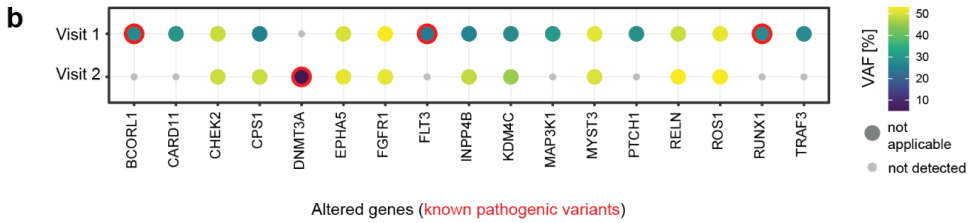
b
Visit 1
Visit 2
BCORL1
CARD11
CHEK2
CPS1
DNMT3A
EPHA5
FGFR1
FLT3
INPP4B
KDM4C
MAP3K1
MYST3
PTCH1
RELN
ROS1
RUNX1
TRAF3
VAF [%]
50
40
30
20
10
not applicable
not detected
Altered genes (known pathogenic variants)

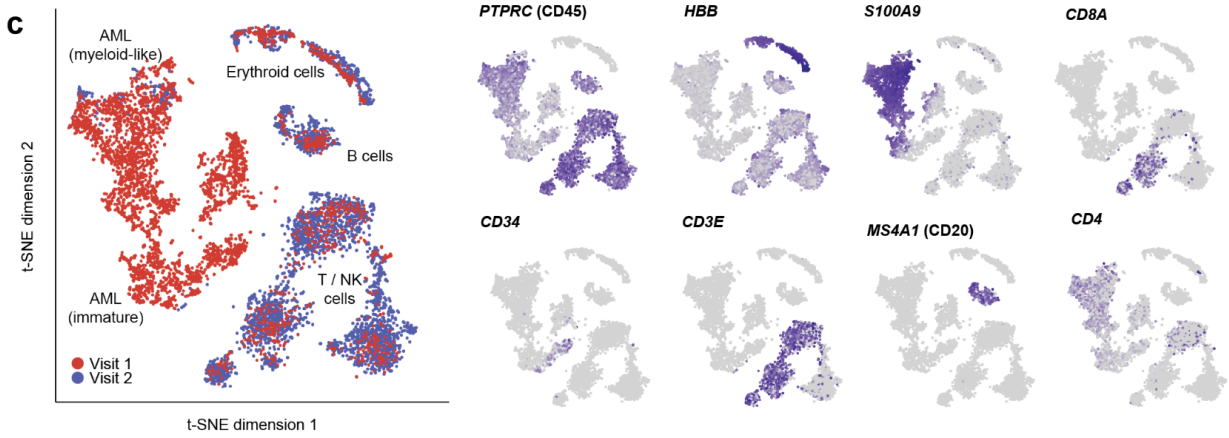
c
AML (myeloid-like)
Erythroid cells
B cells
T / NK cells
AML (immature)
Visit 1
Visit 2
t-SNE dimension 1
t-SNE dimension 2
PTPRC (CD45)
HBB
S100A9
CD8A
CD34
CD3E
MS4A1 (CD20)
CD4

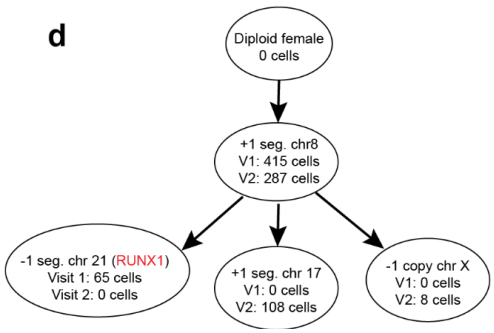
d
Diploid female
0 cells
+1 seg. chr8
V1: 415 cells
V2: 287 cells
-1 seg. chr 21 (RUNX1)
Visit 1: 65 cells
Visit 2: 0 cells
+1 seg. chr 17
V1: 0 cells
V2: 108 cells
-1 copy chr X
V1: 0 cells
V2: 8 cells

Supplementary Figure 5. a: Schematic of the clinical course of patient TP030. **b**: Variant allele frequencies from FoundationOne Heme for genomic alterations detected in at least one patient sample. **c**: t-SNE calculated on the batch-corrected expression values of all cells measured by scRNA-seq (visit 1: 3469 cells, visit 2: 4152 cells). Regions in the t-SNE are annotated with the most abundant cell type, small plots on the side show cell type specific marker gene expression (darker color = higher expression). **d:** Inferred cellular hierarchy based on copy number variations identified by scDNA-seq.

Patient TP030 was initially diagnosed with AML six years before this study. The patient relapsed for the first time after allo-HSCT four years past diagnosis, at which point she was treated with the Flt3-inhibitor midostaurin, leading to a complete remission followed by a second allo-HSCT. After another two years in remission, the patient presented with a second relapse and the first TuPro sample was obtained (**Supplementary Figure 5a**). FoundationOne highlighted the re-emergence of a *FLT3*-ITD mutation, as well as the presence of mutations in *BCORL1, CHEK2* and a splice site mutation in *RUNX1* (**Supplementary Figure 5b**). Based on the *FLT3* mutation, the patient was treated with Gilteritinib after the first visit and achieved a complete remission (**Supplementary Figure 5a**). Interestingly, although the previously observed pathogenic mutations disappeared at the second visit, we observed a low frequency *DNMT3A* R882C mutation emerging at this time point. This mutation persisted at low frequencies even though the patient remained in remission, likely reflecting clonal hematopoiesis. This finding is consistent with a previous study that identified no correlation between disease progression and the persistence of *DNMT3A* mutations [2]. scRNA-seq analysis revealed that the first sample was dominated by AML blasts (>80%) with mostly myeloid-like phenotype and only a small fraction of CD34 positive cells (**Supplementary Figure 5c**). Consistent with the clinical course of the patient, AML blasts were no longer present in the second sample, which was instead composed of a mixture of erythroid cells, B cells and a large fraction of T- and NK cells. Analysis of CNVs by scDNA-seq indicated a gain of a short segment on chromosome 8 in all analyzed cells, thus likely representing a germline variant. An additional clone characterized by loss of one copy of the segment of chromosome 21 where *RUNX1* is located (21q.22) was only detected at visit 1, while two clones characterized by a gain of one segment in chromosome 17 and loss of one copy of the X-chromosome, respectively, were present at the second visit only (**Supplementary Figure 5d**).

TP031

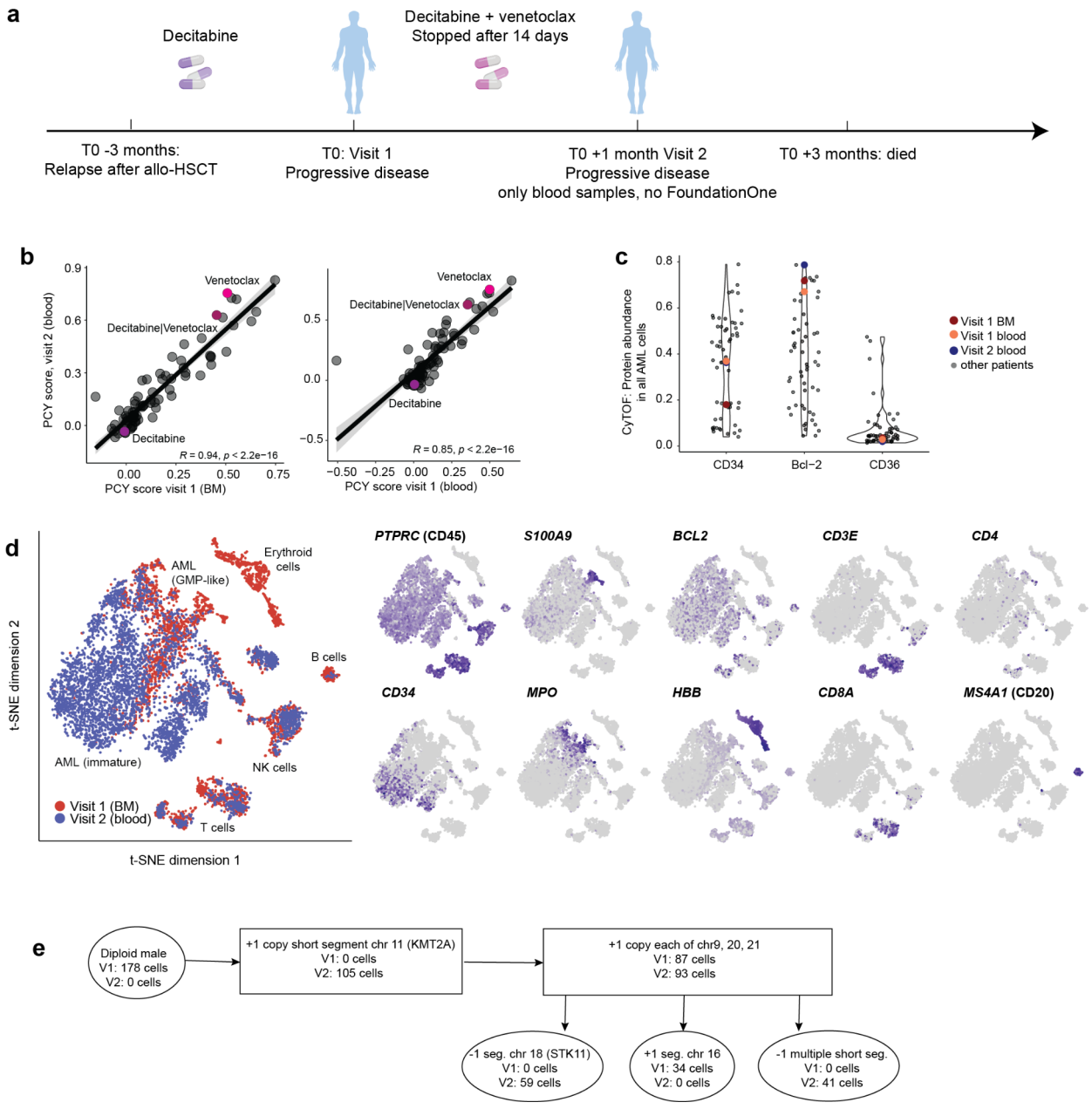

Supplementary Figure 6. a: Schematic of the clinical course of patient TP031. **b**: Correlation of PCY scores between visit 1 and visits 2 and 3, respectively. The colored dots highlight the previous treatment (decitabine) and the treatment following the first visit (decitabine + venetoclax). Lines and shaded areas correspond to a linear regression fit with 95% confidence bands. *P* values (two-sided t-test) and Pearson's *R* are indicated. Data are from three biological replicates (blood and bone marrow samples at visit 1, blood only at visit 2). **c**: Expression of CD34, Bcl-2 and CD36 by CyTOF. Black dots correspond to all samples in the cohort, colored dots mark samples from patient TP031. **d**: t-SNE calculated on the batch-corrected expression values of all cells measured by scRNA-seq (visit 1: 3261 cells, visit 2 (peripheral blood sample): 4648 cells). Regions in the t-SNE are annotated with the most abundant cell type, small plots on the side show cell type specific marker gene expression (darker color = higher expression). **e:** Inferred clonal hierarchy based on copy number variations identified by scDNA-seq.

Patient TP031 was initially diagnosed with *KMT2A* rearranged AML. The patient had been treated by allo-HSCT and prophylactic treatment with decitabine, but eventually relapsed three months prior to the first TuPro visit (**Supplementary Figure 6a**). After the first sampling, the patient received decitabine + venetoclax, however the treatment was stopped after 14 days. A second sample (peripheral blood only) was then analyzed. PCY analysis identified venetoclax-based treatments among the strongest on-target hits in all samples analyzed (**Supplementary Figure 6b**). Consistent with the *ex vivo* sensitivity to Bcl-2 inhibition, CyTOF analysis highlighted high expression of CD34 and Bcl-2 compared to the remainder of the cohort (**Supplementary Figure 6c**), and scRNA-seq identified primarily immature AML blasts with high expression of *CD34* and *BCL2* (**Supplementary Figure 6d**). This was particularly pronounced in the blood sample analyzed at visit 2, which was composed of >80% of mostly HSC-like immature blasts. scDNA-seq analysis highlighted the presence of multiple clones with different CNV patterns, of which some were sample-specific.

Supplementary Figures 7-13

Supplementary Figure 7

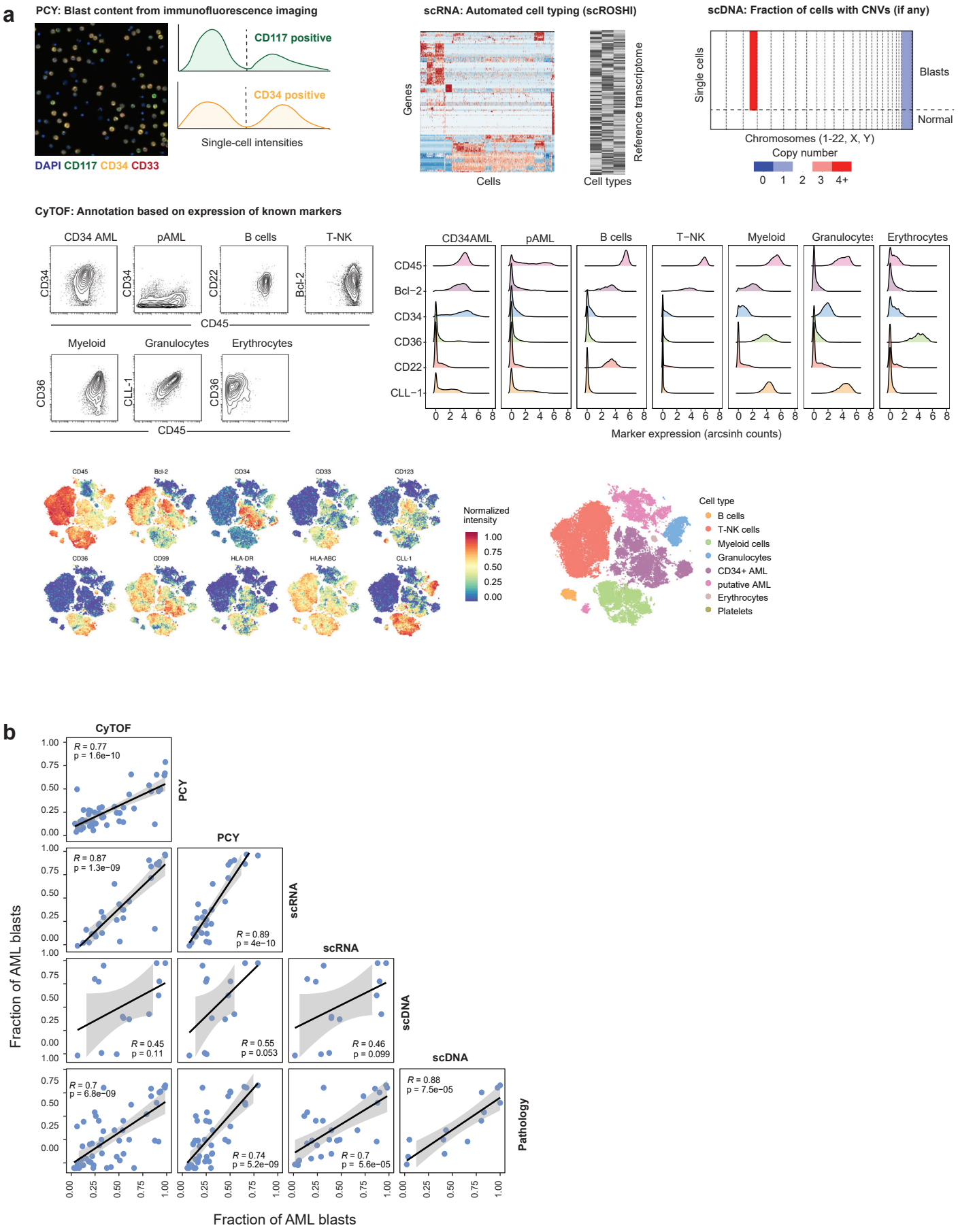

Supplementary Figure 7

Identification of AML blasts across TuPro technologies. **a:** Schematic illustrating the definition of blasts across technologies (see Methods for details). For PCY, it corresponds to the fraction of cells positive for CD34 or CD117. For scRNA, blasts were identified using automated hierarchical cell typing based on reference transcriptomes (**Supplementary Data 13**) as described by Prummer et al [3]. For CyTOF, blasts were defined on the abundance of known markers, primarily CD45 (low) and absence of erythroid markers (putative AML), and additionally CD34 (high) (CD34+ AML). For scDNA, only samples with any CNVs are considered and the blast fraction corresponds to the fraction of cells with CNVs in a panel of disease-relevant genes (**Supplementary Data 3**). **b:** Correlation of blast fractions identified by TuPro technologies and pathology. Pathology refers to bone marrow aspirate cytology (histology if no cytology readout was available) for bone marrow samples and cytology for blood samples. Linear regression lines with 95% confidence bands, Pearson's *R* and corresponding *P* values (two-tailed t-test) are indicated. Sample numbers (biological replicates): CyTOF n = 57; PCY n = 48, scRNA n = 29; Pathology n = 53; scDNA n =14.

Supplementary Figure 8

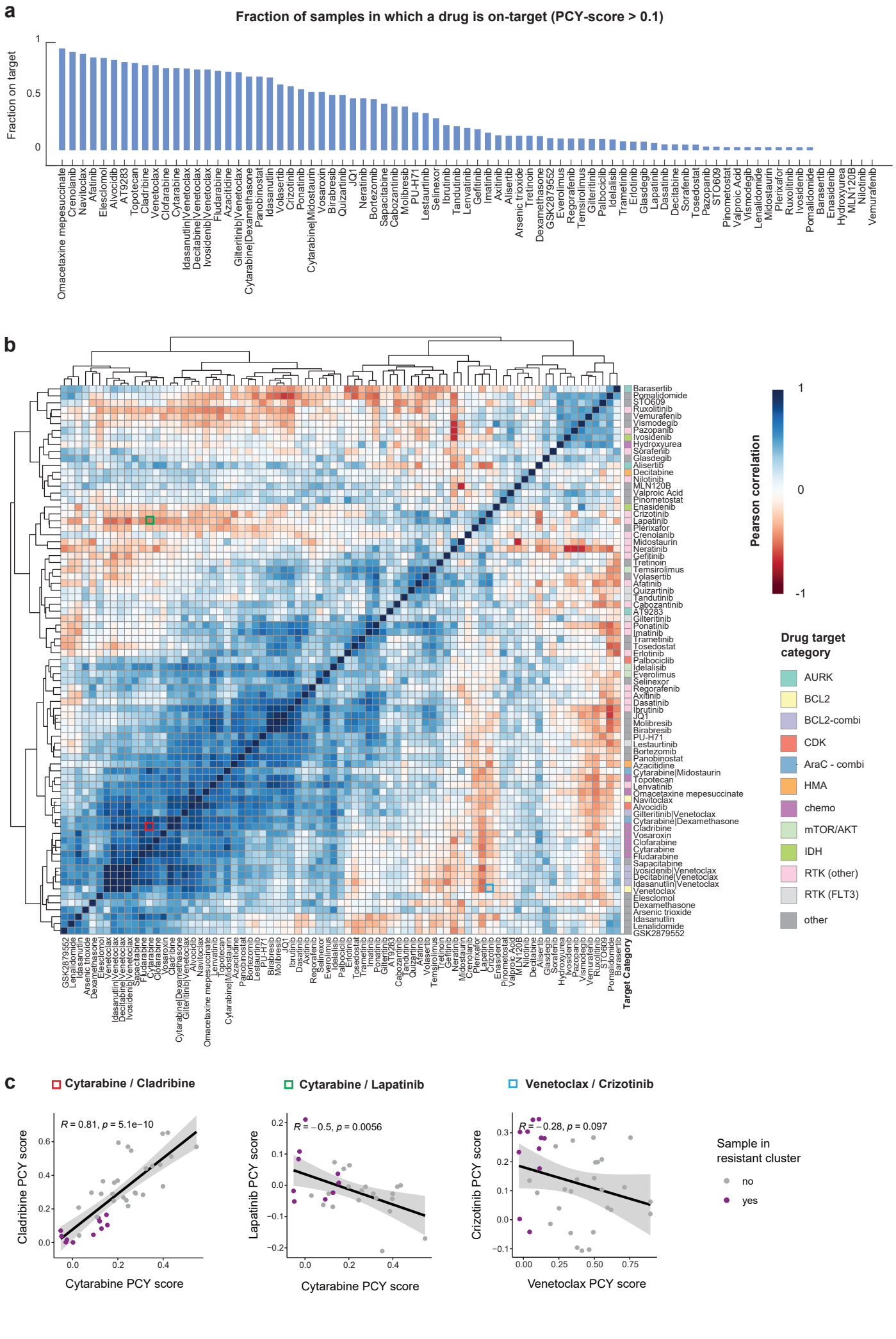

Supplementary Figure 8

PCY-based *ex vivo* drug response landscape of rrAML. **a:** Fraction of samples in which a drug scored on-target (PCY score > 0.1), by drug. **b:** Drug-drug correlation matrix of PCY scores. Drugs are ordered by hierarchical clustering (euclidean distance, complete linkage). Color represents Pearson correlation between each pair of drugs. Manually curated drug target categories are annotated. **c:** Example correlation plots for selected drug-drug pairs, highlighted by colored squares in (b). Purple dots correspond to samples in the chemoresistant cluster (see **Figure 2a**). Linear regression lines with 95% confidence bands, Pearson's *R* and corresponding *P* values (two-sided t-test) are indicated. Data represent 38 samples with > 5% blast content by cytology from 18 patients.

Supplementary Figure 9

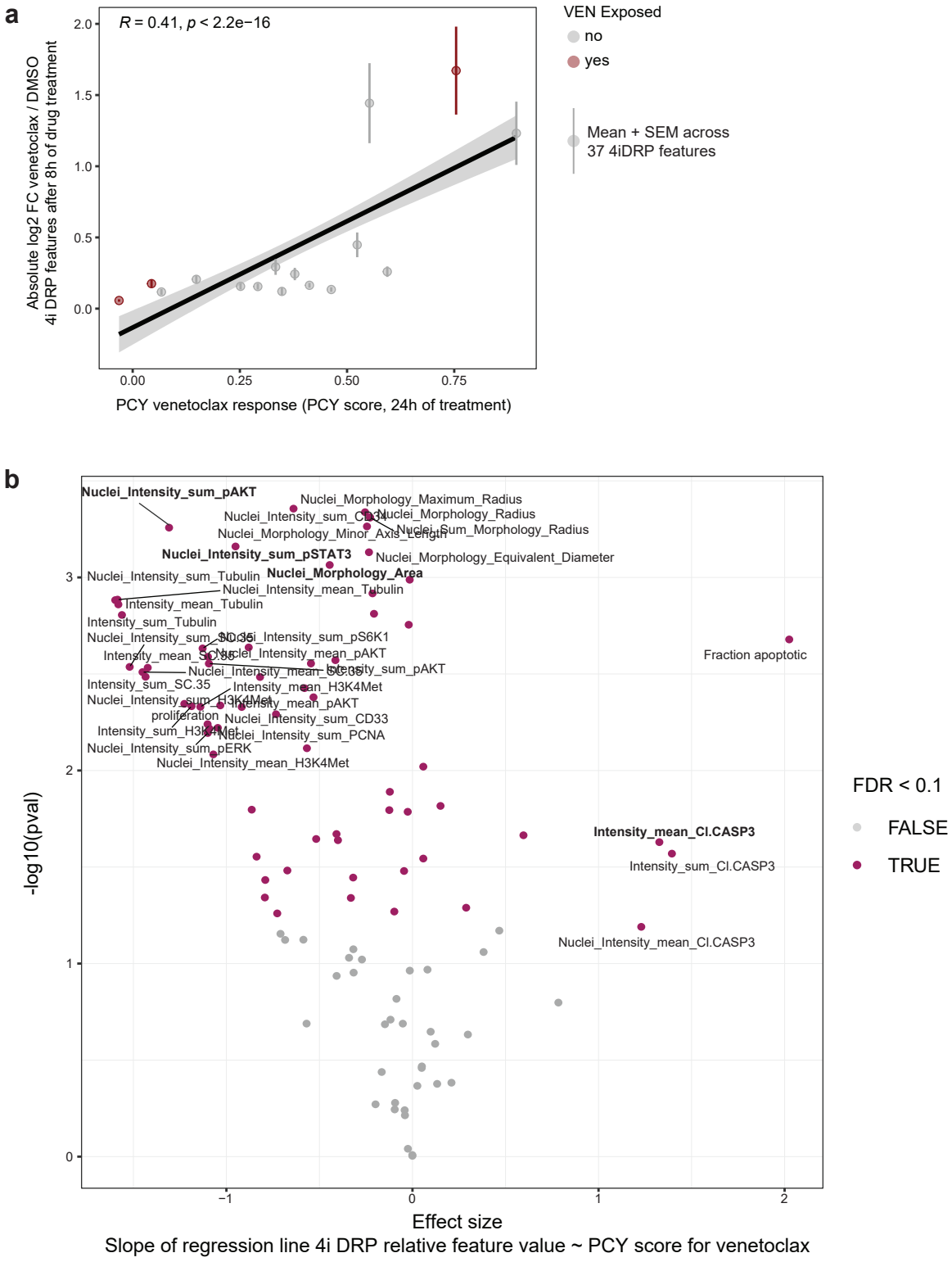

Supplementary Figure 9

Consistency between *ex vivo* responses by PCY and 4i DRP. **a:** Absolute log2 fold changes (FC) comparing VEN to DMSO control across 4i DRP features versus VEN PCY scores. Each dot corresponds to the mean absolute FC across 37 4iDRP features for a single sample, lines correspond to the standard error of the mean, and colors mark VEN exposure at the time of sampling. **b:** Volcano plot for the association of VEN PCY scores and VEN-induced changes in 4i DRP features. The x-axis corresponds to the slope of the regression line with VEN PCY scores as predictor and the DMSO-normalized 4i DRP features as the response variable. The y-axis denotes uncorrected p values of the linear model (two-sided t-test). Red dots denote Benjamini-Hochberg FDR < 0.1. Features shown in **Figure 2d** are highlighted in bold. All data represent 16 samples from 13 patients that had a blast content of > 5% and were measured both by 4i DRP and PCY.

Supplementary Figure 10

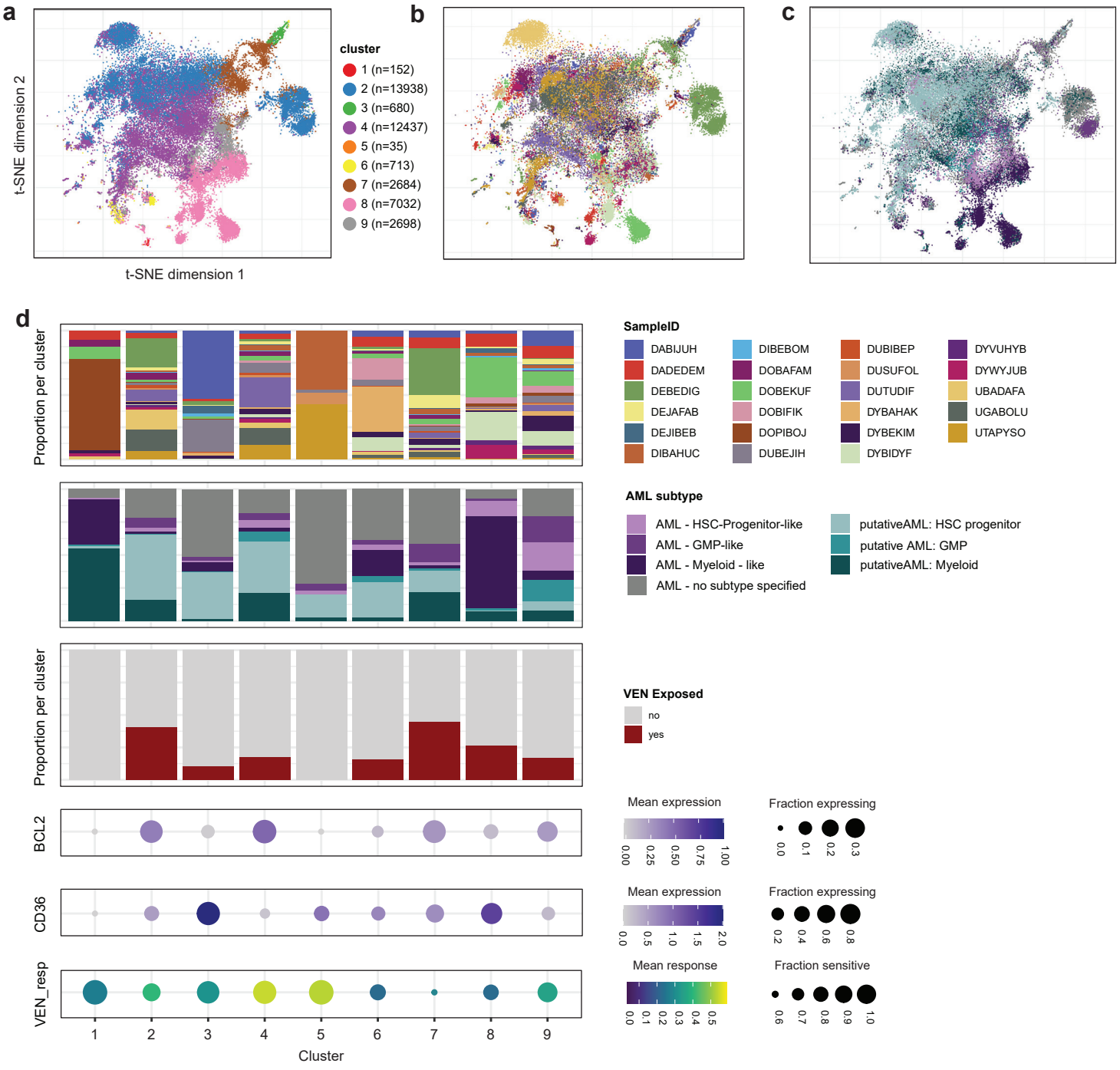

Supplementary Figure 10

A single-cell landscape of rrAML. **a-c:** t-SNE calculated on scRNA expression of 40369 AML cells. **a:** Colored by phenograph cluster assignment, **b:** Colored by sample ID, **c:** Colored by AML subtype (assigned by scROSHI, see **Supplementary Data 13** and Methods). **d:** Characteristics of the clusters shown in (a). From top to bottom: Contribution of each sample ID to each cluster; Fraction of AML subtypes per cluster; Contribution of cells from VEN exposed and non-exposed samples to each cluster; Average *BCL2* and *CD36* expression; VEN sensitivity (PCY score, weighted by relative abundance of cells per sample) per cluster.

Supplementary Figure 11

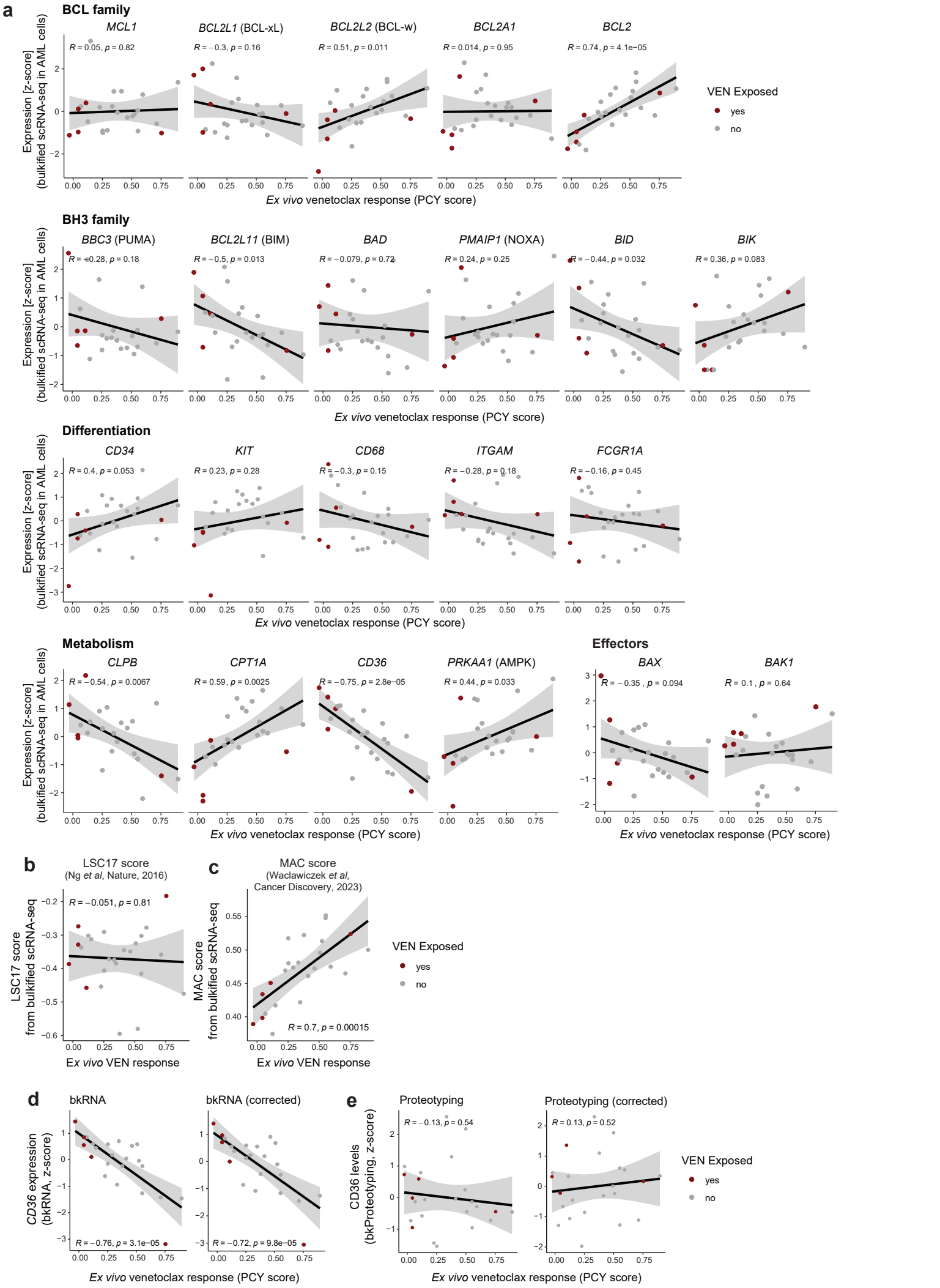

Supplementary Figure 11

Molecular determinants of VEN sensitivity. **a:** Scatterplots of VEN PCY score against gene expression (scRNA-seq, bulkified across all AML cells per sample) for genes with previously reported associations to VEN resistance (see **Figure 3d** and **Supplementary Table 1**). **b,c:** Correlation of PCY-based VEN response and composite biomarkers calculated from bulkified scRNA-seq expression in AML cells. **b:** 17-gene leukemia stem cell (LSC17) score [4], **C:** Mediators of apoptosis combinatorial (MAC) score [5]. **d:** Expression of *CD36* in bulk RNA. Left: z-scored normalized expression values. Right: z-scored normalized expression values after regressing out the effect of blast content. **e**: Abundance of CD36 in bulk proteotyping. Left: normalized protein abundance. Right: z-scored normalized protein abundance after regressing out the effect of blast content. Linear regression line with 95% confidence bands, Pearson's *R* and corresponding *P* values (two-sided t-test) are shown. Sample and patient numbers: a-c: 24 samples from 18 patients; d: 26 samples from 17 patients; e: 25 samples from 12 patients.

Supplementary Figure 12

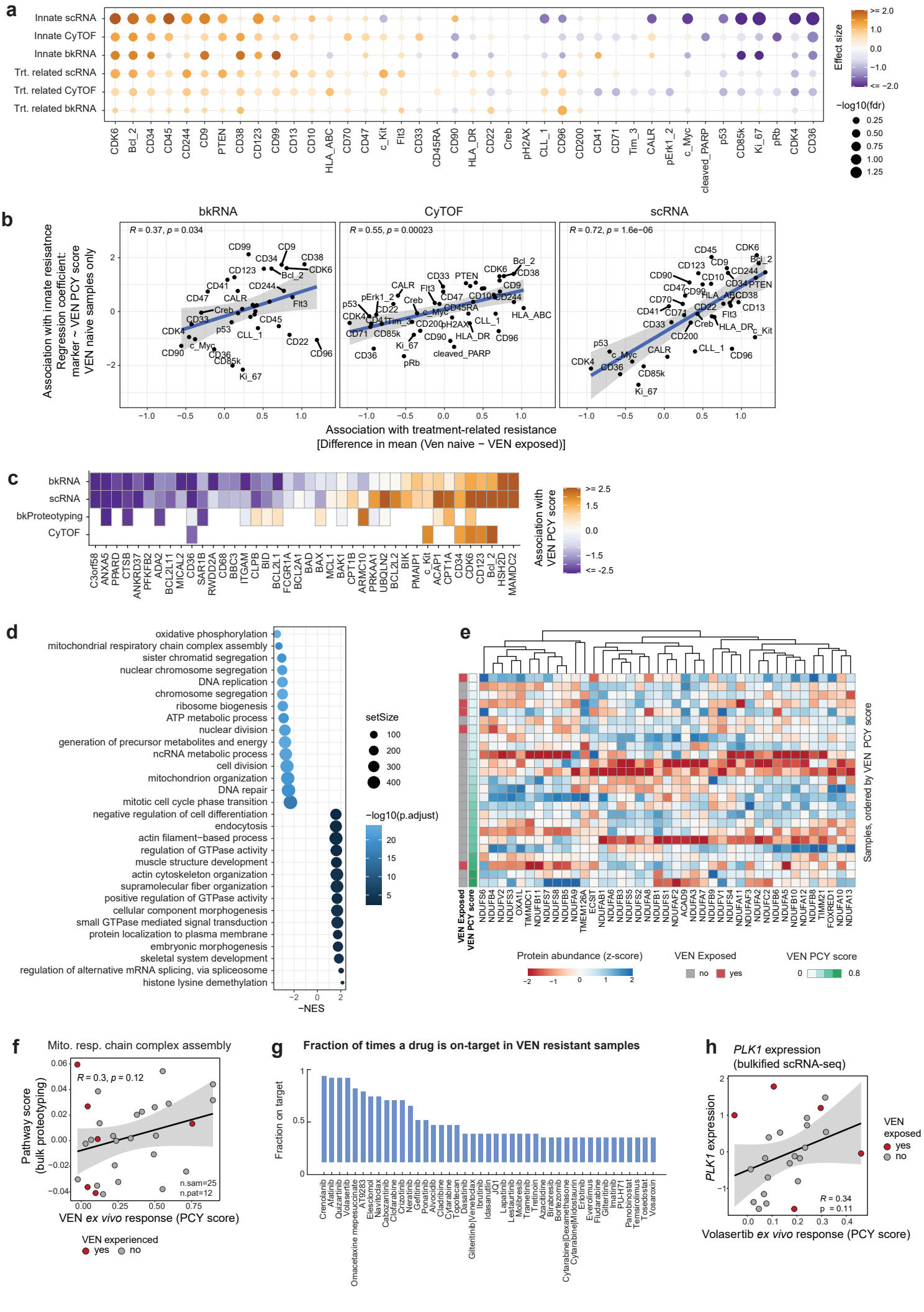

Supplementary Figure 12

Comparison of molecular associations with VEN resistance across technologies. **a-b:** Association of protein / RNA levels with innate and treatment-related resistance to VEN for all markers in the CyTOF panel. Effect size represents the slope of the regression line for innate resistance and the difference in mean between VEN naive and VEN exposed samples for acquired resistance. *P* values obtained from a linear regression and a two-sided Welch's t-test, respectively. CyTOF: n=38 samples from 18 patients; scRNA: n=24 samples from 18 patients; bkRNA: 26 samples from 17 patients. **c:** Association of marker (protein or RNA) levels with VEN PCY score across all samples and 4 technologies. Shown are literature-derived genes known to be involved in VEN resistance, as well as the top 5 associations by technology. Values correspond to the slope of the regression line marker level ~ VEN PCY score **d:** GSEA result using the average association between gene expression in AML cells (scRNA-seq) and innate / acquired VEN resistance to rank genes. Negative enrichment scores indicate association with resistance, and positive scores with sensitivity. **e:** Protein abundances for all detected proteins in the pathway "mitochondrial respiratory chain complex assembly" (GO:GO:0032981). Colors represent z-scored, blast content-corrected protein abundances. Samples are ordered by VEN PCY score, proteins are rendered by hierarchical clustering (Euclidean distance, complete linkage). **f:** Pathway score (singscore, [6]) for the proteins shown in (e), associated with VEN *ex vivo* response. Data in (e) and (f) represent 29 samples from 12 patients. **g:** Fraction of VEN resistant samples (n=12) that were ex vivo sensitive (1-RBF > 0.1) per drug. Only drugs to which at least 5 samples were sensitive are shown. **h:** Correlation between ex vivo response to volasertib and expression (bulkified scRNA-seq) of the drug's target *PLK1*. b,f,h: Regression line with 95% confidence bands, Pearson's *R* and *P* value (two-sided t-test) are indicated. All analyses were performed for samples with > 5% blast content. In a,b, and d, samples from patients that were treated with venetoclax in previous treatment lines were excluded.

Supplementary Figure 13

a BEAT AML − full cohort (patients < 18 years excluded)

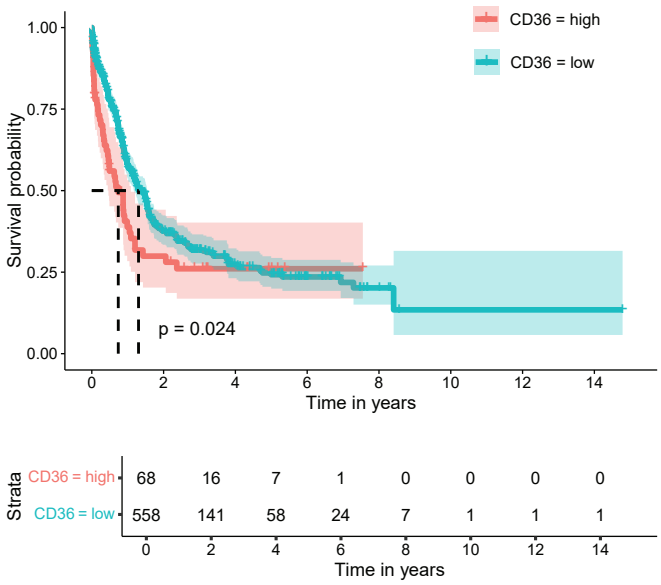

b BEAT AML − newly diagnosed only (patients < 18 years excluded)

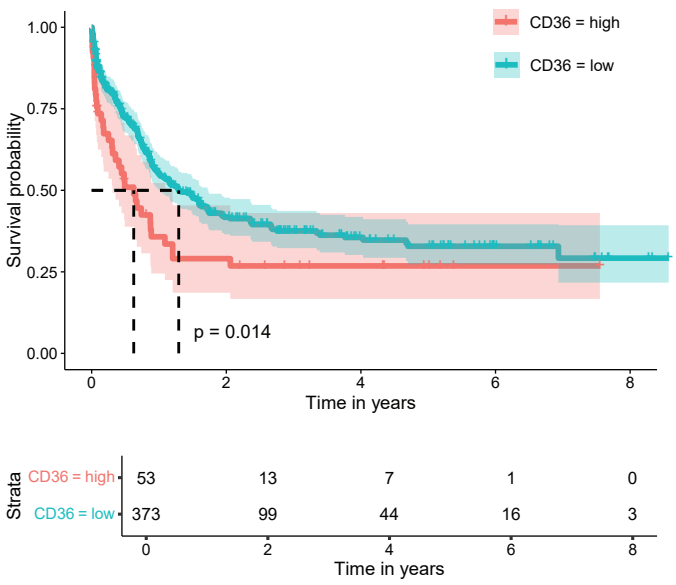

Supplementary Figure 13

Kaplan-Meier curves for patients in the BEAT-AML cohort, stratified by CD36 expression level (bulk RNA-seq). P value from a log-rank test is indicated. **a,** including all samples from patients > 18 years old (n=626), **b,** only including newly diagnosed patients > 18 years old (n=426). Patient numbers per 2-year interval are indicated. Lines indicate the Kaplan-Meier survival probability estimate, estimate, shaded areas correspond to the 95% confidence interval and tick marks represent censored events.

Supplementary Table 1: Summary of known venetoclax resistance mechanisms involving altered gene expression

Category	Protein (*Gene*)	Mechanism of / association with resistance	References
BCL2 family	BCL2	Decreased ratio of BCL2 / other BCL family members	[5,7]
	MCL1	upregulation	[7–10]
	BCL-xL (*BCL2L1*)	upregulation	[7,10]
	BCL-w (*BCL2L2*)		
	BCL2A1	upregulation	[11]
BH3 proteins (sensitizers)	NOXA (*PMAIP1*)	Loss or downregulation by TP53 loss	[12,13]
BH3 proteins (sensitizers)	BIK		
BH3 proteins (sensitizers)	BIM (*BCL2L11*)		
BH3 proteins (activators)	BID		
BH3 proteins (activators)	BAD		
BH3 proteins (activators)	PUMA (*BBC3*)	Downregulation by TP53 loss	[13]
Effectors	BAX, BAK (*BAK1*)	loss or downregulation by TP53 loss	[12,13]
Metabolism	CPT1A	Upregulation	[14]
	CD36	Upregulation	[14–16]
Mitochondrial structure and function	AMPK (*PRKAA1*)	Upregulation leading to increased oxphos	[17]
Mitochondrial structure and function	CLPB	upregulation	[12]

Differentiation	CD34	down	5 18–20
	Monocytic markers e.g. CD68, CD64 (*FCGR1A*), ITGAM, KIT	up	

Supplementary References

1. Chou, W.-C. *et al.* Persistence of mutant isocitrate dehydrogenase in patients with acute myeloid leukemia in remission. *Leukemia* **26**, 527–529 (2012).
2. Debarri, H. *et al.* IDH1/2 but not DNMT3A mutations are suitable targets for minimal residual disease monitoring in acute myeloid leukemia patients: a study by the Acute Leukemia French Association. *Oncotarget* **6**, 42345–42353 (2015).
3. Prummer, M. *et al.* scROSHI: robust supervised hierarchical identification of single cells. *NAR Genom Bioinform* **5**, lqad058 (2023).
4. Ng, S. W. K. *et al.* A 17-gene stemness score for rapid determination of risk in acute leukaemia. *Nature* **540**, 433–437 (2016).
5. Waclawiczek, A. *et al.* Combinatorial BCL2 Family Expression in Acute Myeloid Leukemia Stem Cells Predicts Clinical Response to Azacitidine/Venetoclax. *Cancer Discov.* **13**, 1408–1427 (2023).
6. Foroutan, M. *et al.* Single sample scoring of molecular phenotypes. *BMC Bioinformatics* **19**, 404 (2018).
7. Konopleva, M. *et al.* Efficacy and Biological Correlates of Response in a Phase II Study of Venetoclax Monotherapy in Patients with Acute Myelogenous Leukemia. *Cancer Discov.* **6**, 1106–1117 (2016).
8. Zhang, Q. *et al.* Activation of RAS/MAPK pathway confers MCL-1 mediated acquired resistance to BCL-2 inhibitor venetoclax in acute myeloid leukemia. *Signal Transduction and Targeted Therapy 2022 7:1* **7**, 1–13 (2022).
9. Yecies, D., Carlson, N. E., Deng, J. & Letai, A. Acquired resistance to ABT-737 in lymphoma cells that up-regulate MCL-1 and BFL-1. *Blood* **115**, 3304–3313 (2010).
10. Choudhary, G. S. *et al.* MCL-1 and BCL-xL-dependent resistance to the BCL-2 inhibitor ABT-199 can be overcome by preventing PI3K/AKT/mTOR activation in lymphoid malignancies. *Cell Death Dis.* **6**, e1593 (2015).
11. Zhang, H. *et al.* Integrated analysis of patient samples identifies biomarkers for venetoclax efficacy and combination strategies in acute myeloid leukemia. *Nature cancer* **1**, 826 (2020).
12. Chen, X. *et al.* Targeting Mitochondrial Structure Sensitizes Acute Myeloid Leukemia to Venetoclax Treatment. *Cancer Discov.* **9**, 890–909 (2019).
13. Nechiporuk, T. *et al.* The TP53 Apoptotic Network Is a Primary Mediator of Resistance to BCL2 Inhibition in AML Cells. *Cancer Discov.* **9**, 910–925 (2019).
14. Stevens, B. M. *et al.* Fatty acid metabolism underlies venetoclax resistance in acute myeloid leukemia stem cells. *Nature Cancer 2020 1:12* **1**, 1176–1187 (2020).
15. T, Z. *et al.* Apolipoprotein C2 - CD36 Promotes Leukemia Growth and Presents a Targetable Axis in Acute Myeloid Leukemia. *Blood cancer discovery* **1**, 198–213 (2020).
16. Zhang, Y. *et al.* IL-6 promotes chemoresistance via upregulating CD36 mediated fatty acids uptake in acute myeloid leukemia. *Exp. Cell Res.* **415**, 113112 (2022).
17. Guiè, R. *et al.* Mitochondrial Reprogramming Underlies Resistance to BCL-2 Inhibition in Lymphoid Malignancies. *Cancer Cell* **36**, 369–384 (2019).
18. Pei, S. *et al.* Monocytic Subclones Confer Resistance to Venetoclax-Based Therapy in Acute Myeloid Leukemia Patients. *Cancer Discov.* **10**, 536 (2020).
19. Kuusanmäki, H. *et al.* Ex vivo venetoclax sensitivity testing predicts treatment response in acute myeloid leukemia. *Haematologica* (2022) doi:10.3324/HAEMATOL.2022.281692.
20. Zeng, A. G. X. *et al.* A cellular hierarchy framework for understanding heterogeneity and predicting drug response in acute myeloid leukemia. *Nature Medicine 2022 28:6* **28**, 1212–1223 (2022).
21. Döhner, H. *et al.* Diagnosis and management of AML in adults: 2022 recommendations from an international expert panel on behalf of the ELN. *Blood* **140**, 1345–1377 (2022).
22. Čuklina, J. *et al.* Diagnostics and correction of batch effects in large-scale proteomic studies: a tutorial. *Mol. Syst. Biol.* **17**, e10240 (2021).